J|A|C|S
ARTICLES
Published on Web 04/27/2006

Synthesis, Photochemistry, and Electrochemistry of Single-Wall Carbon Nanotubes with Pendent Pyridyl Groups and of Their Metal Complexes with Zinc Porphyrin. Comparison with Pyridyl-Bearing Fullerenes

Mercedes Alvaro,[†] Pedro Atienzar,[†] Pilar de la Cruz,[‡] Juan L. Delgado,[‡] Vincent Troiani,[‡] Hermenegildo Garcia,*[,†] Fernando Langa,*[,‡] Amit Palkar,[§] and Luis Echegoyen*[,§]

Contribution from the Instituto de Tecnología Química CSIC-UPV, Universidad Politécnica de Valencia, 46022-Valencia, Spain, Facultad Ciencias del Medio Ambiente, Universidad de Castilla-La Mancha, 45071-Toledo, Spain, and Department of Chemistry, Clemson University, Clemson, South Carolina 29634

Received November 14, 2005; E-mail: hgarcia@qim.upv.es; flanga@amb-to.uclm.es; luis@clemson.edu

Abstract: A soluble, functionalized **Py-SWNT** has been synthesized and characterized by solution ^{1}H and ^{13}C NMR, FT-Raman, and electron microscopy. Experimental data indicate that **Py-SWNT** has short tubes with pentyl esters at the tips and pyridyl isoxazolino units along the walls. The synthesis of **Py-SWNT** is based on a 1,3-dipolar cycloaddition of a nitrile oxide on the SWNT walls, similar to 1,3-dipolar cycloadditions that are common for fullerene functionalization. The resulting **Py-SWNT** forms a complex with a zinc porphyrin (**ZnPor**) in a way similar to that reported for pyridyl-functionalized [60]-fullerenes. Formation of this metal−ligand complex was firmly established by a detailed electrochemical study. However, in contrast to the behavior observed for the **ZnPor/Py-C_{60}** complex, photochemical excitation of the complex between **ZnPor/Py-SWNT** does not lead to electron transfer with the generation of charge-separated states. Fluorescence and laser flash studies indicate that the main process is energy transfer from the singlet **ZnPor** excited state to the **Py-SWNT** with observation of emission from **Py-SWNT**. Triplet **ZnPor** excited-state quenching by **Py-SWNT** is only observed in polar solvents such as DMF, but not in benzonitrile.

Introduction

The novel and unique electronic properties[1] exhibited by fullerenes and carbon nanotubes make them excellent candidates for the development of optoelectronic and photovoltaic devices.[2] Currently, there is considerable interest in studying the photophysical properties of single-wall carbon nanotube (SWNT) derivatives obtained by covalent[3] and noncovalent[4] functionalization, with the aim of obtaining photoresponsive materials.[5] The aim of this research is to search for long-lived charge-separated states that could be used in the field of photovoltaics.[6]

Many of the photoactive dyads that have been previously studied consist of a metalloporphyrin−fullerene donor−acceptor (D−A) system[7] connected through a spacer. These dyads differ from one another in the nature of the spacer used for attachment and/or the point of attachment of the porphyrin to the fullerene core. In these systems, upon excitation with appropriate wavelength of light, the metalloporphyrin acts as the energy/electron donor substructure while the fullerene acts as the

[†] Universidad Politécnica de Valencia.
[‡] Universidad de Castilla-La Mancha.
[§] Clemson University.

(1) (a) *Carbon Nanotubes: Synthesis, Structure and Applications*; Dresselhaus, M. S., Dresselhaus, G., Avouris, Ph., Eds.; Springer Publishing: New York, 2001. (b) Reich, S.; Thomsen, C.; Maultzsch, J. *Carbon Nanotubes: Basic Concepts and Physical Properties*; Wiley-VCH: Weinheim, 2004.
(2) (a) Hirsch, A. *Angew. Chem., Int. Ed.* **2002**, *41*, 1853. (b) Bahr, J. L.; Tour, J. M. *J. Mater. Chem.* **2002**, *12*, 1952. (c) Niyogi, S.; Hamon, M. A.; Hu, H.; Zhao, B.; Bhomwik, P.; Sen, R.; Itkis, M. E.; Haddon, R. C. *Acc. Chem. Res.* **2002**, *35*, 1105. (d) Sun, Y.-P.; Fu, K.; Lin, Y.; Huang, W. *Acc. Chem. Res.* **2002**, *35*, 1096. (e) Banerjee, S.; Kahn, M. G. C.; Wang, S. S. *Chem.-Eur. J.* **2003**, *9*, 1898. (f) Tasis, D.; Tagmatarchis, N.; Georgakilas, V.; Prato, M. *Chem.-Eur. J.* **2003**, *9*, 4000. (g) Dyke, C. A.; Tour, J. M. *Chem.-Eur. J.* **2004**, *10*, 812.
(3) (a) Georgakilas, V.; Kordatos, K.; Prato, M.; Guldi, D. M.; Holzinger, M.; Hirsch, A. *J. Am. Chem. Soc.* **2002**, *124*, 760. (b) Dyke, C. A.; Tour, J. M. *J. Am. Chem. Soc.* **2003**, *125*, 1156. (c) Holzinger, M.; Abraham, J.; Whelan, P.; Graupner, R.; Ley, L.; Hennrich, F.; Kappes, M.; Hirsch, A. *J. Am. Chem. Soc.* **2003**, *125*, 8566. (d) Murakami, H.; Nomura, T.; Nakashima, N. *Chem. Phys. Lett.* **2003**, *378*, 481. (e) Guldi, D. M.; Marcaccio, M.; Paolucci, D.; Paolucci, F.; Tagmatarchis, N.; Tasis, D.; Vazquez, E.; Prato, M. *Angew. Chem., Int. Ed.* **2003**, *42*, 4206.
(4) (a) Star, A.; Steuerman, D. W.; Heath, J. R.; Stoddart, J. F. *Angew. Chem., Int. Ed.* **2002**, *41*, 2508. (b) Fukushima, T.; Kosaka, A.; Ishimura, Y.; Yamamoto, T.; Takigawa, T.; Ishii, N.; Aida, T. *Science* **2003**, *300*, 2072. (c) Sun, J.; Gao, L.; Iwasa, M. *Chem. Commun.* **2004**, 832.
(5) (a) Fujiwara, A.; Matsuoka, Y.; Suematsu, H.; Ogawa, N.; Miyano, K.; Kataura, H.; Maniwa, Y.; Suzuki, S.; Achiba, Y. *Jpn. J. Appl. Phys.* **2001**, *40*, L1229. (b) Freitag, M.; Martin, Y.; Misewich, J. A.; Martel, R.; Avouris, Ph. *Nano Lett.* **2003**, *3*, 1067. (c) Cao, L.; Chen, H.; Wang, M.; Sun, J.; Zhang, X.; Kong, F. *J. Phys. Chem. B* **2002**, *106*, 8971.
(6) *Electron Transfer in Chemistry*; Balzani, V., Ed.; Wiley-VCH: Weinheim, 2001; Vols. I−V.
(7) (a) El-Khouly, M. E.; Ito, O.; Smith, P. M.; D'Souza, F. *J. Photochem. Photobiol., C* **2004**, *5*, 79. (b) Wilson, S. R.; Macmahon, S.; Tat, F.; Jarowski, P. D.; Schuster, D. I. *Chem. Commun.* **2003**, 226. (c) Tat, F. T.; Zhou, Z.; Song, S. M. F.; Rheingold, A. R.; Echegoyen, L.; Schuster, D. I.; Wilson, S. R. *J. Org. Chem.* **2004**, *69*, 4602. (d) Hauke, F.; Swartz, A.; Guldi, D. M.; Hirsch, A. *J. Mater. Chem.* **2002**, *12*, 2088. (e) Solladié, N.; Walther, M. E.; Gross, M.; Figueira-Duarte, T. M.; Bourgogne, C.; Nierengarten, J.-F. *Chem. Commun.* **2003**, 2412. (f) Souza, F. D.; Smith, P. M.; Gadde, S.; McCarty, A. L.; Kullman, M. J.; Zandler, M. E.; Itou, M.; Araki, Y.; Ito, O. *J. Phys. Chem. B* **2004**, *108*, 11333.

 10.1021/ja057742i CCC: $33.50

corresponding acceptor moiety. Recently, it has been reported that SWNT and metal porphyrins may spontaneously self-assemble to form complexes in the ground state.[8] Prato, Guldi, and co-workers have recently reported donor−acceptor nanoassemblies of soluble SWNT containing covalently bonded benzenesulfonate anions interacting through Coulombic forces with cationic porphyrins.[9] Some of these systems have already been used to construct photovoltaic cells.[10]

The objective of the present work is to compare and contrast the interaction of **ZnPor** with pyridyl-functionalized fullerenes (**Py-C_{60}**) and SWNT (**Py-SWNT**).

We present here an approach for sidewall SWNT functionalization, which is very similar to one that has already been used for fullerenes.[11] It is well known that metalloporphyrins interact with pyridyl nitrogens through an apical coordinative bond between the porphyrin transition metal atom and the pyridyl ligand. Covalent attachment of the pyridyl ligand to the graphene walls of SWNT should, in principle, serve to establish a similar interaction with the metalloporphyrin. In fact, to provide a valid model for comparison with the SWNT, we have also studied the same type of supramolecular complexation using an analogue [60]fullerene derivative as a reference.

For the synthesis of the SWNT covalently linked to a pyridyl group, we have used the 1,3-dipolar cycloaddition reaction of a nitrile oxide to SWNT. Recently, it has been shown that cycloaddition of nitrile oxides to SWNT is theoretically possible, although the reaction is not as exothermic as other types of 1,3-dipolar cycloadditions.[12] In fact, the formation of several pyrrolidino-SWNT derivatives by cycloaddition of azomethine ylides to SWNT has already been described.[9a] Moreover, we have recently demonstrated that cycloaddition of nitrile imines to SWNT to form pyrazolino-SWNT derivatives is possible.[13]

The isoxazolino-SWNT described in this work is doubly functionalized: at the tips with multiple alkyl chains to provide sufficient solubility in organic solvents and at the sidewalls with 4-pyridylisoxazoline rings to coordinate the metallo-porphyrin to the pyridyl group. The length of the SWNT employed here is short enough to ensure excellent solubility properties in organic solvents upon covalent functionalization of the tips.

Results and Discussion

The synthesis of chemically modified **Py-SWNT** was carried out as indicated in Scheme 1.

Scheme 1. Synthetic Route for the Preparation of **Py-SWNT**

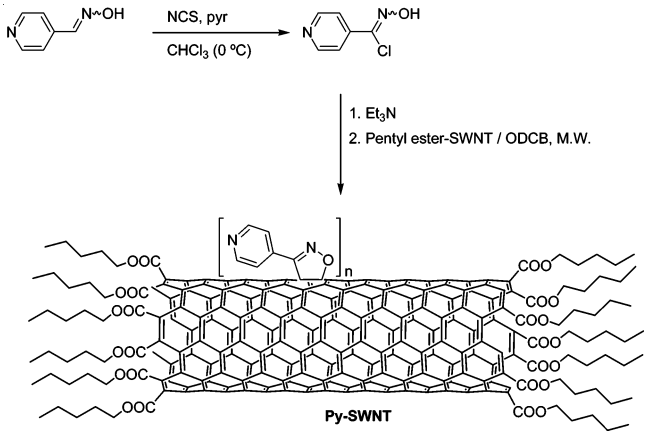

The 4-pyridyl isoxazolino-SWNT (**Py-SWNT**) was synthesized starting from 4-pyridylcarboxaldehyde oxime[14] by reaction with *N*-chlorosuccinimide (NCS) at 0 °C in the presence of a small amount of pyridine (pyr) using anhydrous chloroform as solvent. After the addition of NCS, the reaction was stirred for 15 min at room temperature, the solvent was evaporated, and a solution of the **pentyl ester-SWNT**[15] and triethylamine in *o*-dichlorobenzene (ODCB) was added. **Pentyl ester-SWNTs** were obtained from commercial HiPco SWNT by treatment with 1 M HNO_3 and subsequent esterification of the carboxy groups, formed in the oxidation process, with pentanol. The HNO_3 treatment was optimized to provide SWNT sufficiently short in length (vide infra the corresponding TEM images) to provide excellent solubility of the derivatives. The reaction mixture containing **pentyl ester-SWNT** and nitrile oxide was irradiated in a focused microwave oven at 150 W for 45 min to afford the isoxazolino **Py-SWNT**. The solvent was evaporated, and the solid residue was purified by exhaustive washings with different mixtures of solvents, chloroform/water, chloroform/diethyl ether, and chloroform/pentane.

The chemically modified **Py-SWNTs** were characterized by analytical and spectroscopic methods, all data being consistent with the proposed structure. TEM images of **Py-SWNT** show the typical morphology of the single-walled carbon nanotubes (Figure 1). It can be seen that the most salient feature of the functionalized **Py-SWNT** is the short length dimensions in the range of hundreds of nanometers while the tube morphology is still preserved and aggregation reduced.

The ^{1}H NMR spectrum of isoxazolino **Py-SWNT** (Figure 2) shows two broad signals at around 8.6 and 7.3 ppm corresponding to the protons of the pyridyl group, similar to those observed for [60]fullerene derivative **Py-C_{60}**.[16] The peaks corresponding to the *n*-pentyl chains are also observed as broad signals between 3.5 and 0.5 ppm, similar to the spectrum of **pentyl ester-SWNT**.

The FT-IR spectrum of **Py-SWNT** exhibits the stretching vibration of the C═O esters at 1700 cm^{-1}, while the band at 1630 cm^{-1} can be assigned to the pyridyl ring stretching.

The UV−vis spectrum of isoxazolino **Py-SWNT** shows a continuous absorption with decreasing absorbance toward longer

(8) (a) Murakami, H.; Nomura, T.; Nakashima, N. *Chem. Phys. Lett.* **2003**, *378*, 481. (b) Li, H.; Zhou, B.; Lin, Y.; Gu, L.; Wang, W.; Fernando, K. A. S.; Kumar, S.; Allard, L. F.; Sun, Y.-P. *J. Am. Chem. Soc.* **2004**, *126*, 1014. (c) Guldi, D. M.; Taieb, H.; Rahman, G. M. A.; Tagmatarchis, N.; Prato, M. *Adv. Mater.* **2005**, *17*, 871. (d) Satake, A.; Miyajima, Y.; Kobuke, Y. *Chem. Mater*. **2005**, *17*, 716. (e) Chen, J.; Collier, C. P. *J. Phys. Chem. B* **2005**, *109*, 7605.

(9) (a) Guldi, D. M.; Rahman, G. M. A.; Ramey, J.; Marcaccio, M.; Paolucci, D.; Paolucci, F.; Qin, S.; Ford, W. T.; Balbinot, D.; Jux, N.; Tagmatarchis, N.; Prato, M. *Chem. Commun.* **2004**, *18*, 2034. (b) Guldi, D. M.; Rahman, G. M. A.; Jux, N.; Tagmatarchis, N.; Prato, M. *Angew. Chem., Int. Ed.* **2004**, *43*, 5526. (c) Guldi, D. M.; Rahman, G. M. A.; Prato, M.; Jux, N.; Qin, S.; Ford, W. T. *Angew. Chem., Int. Ed.* **2005**, *44*, 2015.

(10) (a) Imahori, H.; Fukuzumi, S. *Adv. Funct. Mater.* **2004**, *14*, 525. (b) Hasobe, T.; Kashiwagi, Y.; Absalom, M. A.; Sly, J.; Hosomizu, K.; Crossley, M. J.; Imahori, H.; Kamat, P. V.; Fukuzumi, S. *Adv. Mater.* **2004**, *16*, 975. (c) Imahori, H.; Kimura, M.; Hosomizu, K.; Fukuzumi, S. *J. Photochem. Photobiol., A* **2004**, *166*, 57.

(11) El-Kouly, M. E.; Ito, O.; Smith, P. M.; D'Souza, F. *J. Photochem. Photobiol., C* **2004**, *5*, 79.

(12) Lu, X.; Tian, F.; Wang, N.; Zhang, Q. *J. Am. Chem. Soc.* **2003**, *125*, 10459.

(13) Alvaro, M.; Atienzar, P.; de la Cruz, P.; Delgado, J. L.; García, H.; Langa, F. *J. Phys. Chem. B* **2004**, *108*, 12691.

(14) Furniss, B. S.; Hannaford, A. J.; Smith, P. W. G.; Tatchell, A. R. *Vogel's Textbook of Practical Organic Chemistry*; John Wiley & Sons: New York, 1989.

(15) Alvaro, M.; Atienzar, P.; de la Cruz, P.; Delgado, J. L.; García, H.; Langa, F. *Chem. Phys. Lett.* **2004**, *386*, 342.

(16) de la Cruz, P.; Espíldora, E.; González-Cortés, A.; de la Hoz, A.; Langa, F.; López-Arza, V. *J. Org. Chem.* **2000**, *65*, 8675.

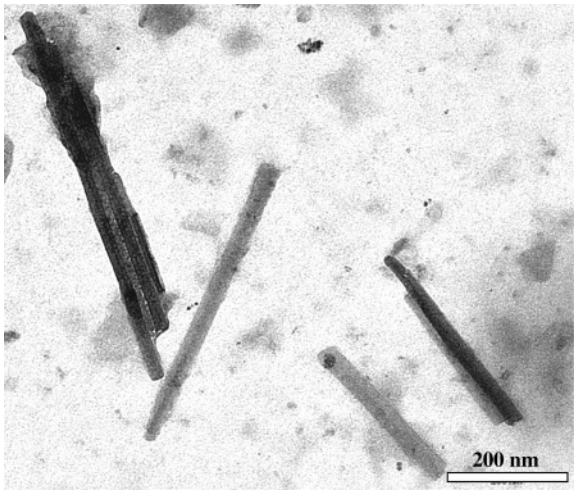

Figure 1. Representative TEM image showing the length and agglomeration of **Py-SWNT**.

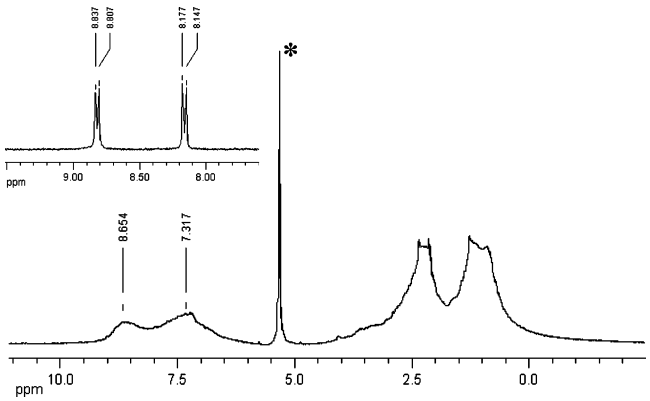

Figure 2. ^{1}H NMR spectra of compounds **Py-SWNT**, in CD_2Cl_2, and **Py-C_{60}** (inset) in $CDCl_3$. The signal due to the solvent has been marked with an asterisk.

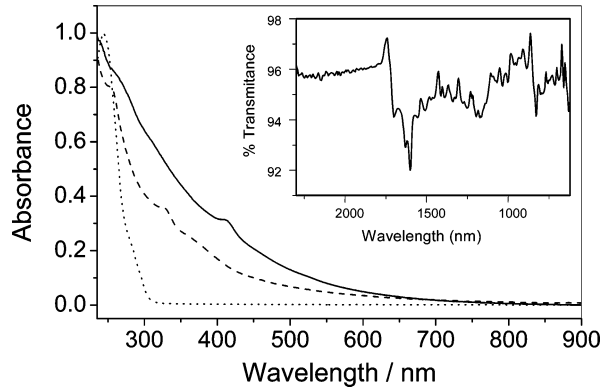

Figure 3. Normalized UV−vis spectra of **Py-SWNT** (−), 4-pyridylcarboxaldehyde oxime (·····), and **pentyl ester-SWNT** (− − −) measured in dichloromethane. The inset shows an expansion of the IR spectrum of **Py-SWNT**.

wavelengths. It shows an absorption maximum at 233 nm and a weak band at 412 nm (Figure 3). The small peak appearing at 412 nm may due to the lateral functionalization with the isoxazoline linker similar to what is observed for the corresponding functionalized fullerene.

Raman spectroscopy is a very important tool to characterize SWNTs.[17] Typically three peaks are observed, one of them appearing around 1600 cm^{-1} that corresponds to the tangential vibration band, which usually decreases in intensity upon chemical modification. A second peak around 1340 cm^{-1} corresponds to defects in the graphene walls and increases in intensity upon chemical functionalization of the graphene walls. The third peak appears in the 100−300 cm^{-1} and is considered specific for single-walled nanotubes, and is related to the radial "breathing" of the tube skeleton.

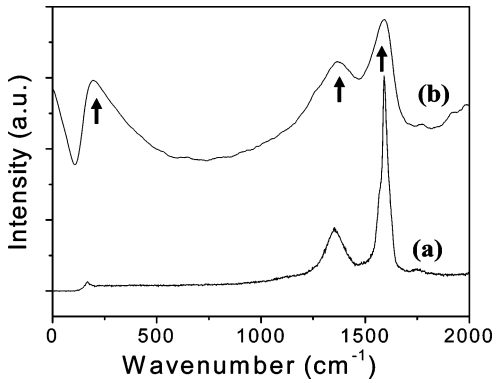

Figure 4. FT-Raman spectra of (a) **pentyl ester-SWNT** and (b) **Py-SWNT**.

Figure 4 shows the Raman spectrum of pyridyl isoxazolino **Py-SWNT** as compared to that of **pentyl ester-SWNT**. This figure shows the relative changes in the intensity of the peaks at 1600 and 1340 cm^{-1}, respectively. As reported,[18] the relative intensity variations of these two peaks from **pentyl ester-SWNT** to **Py-SWNT** are in agreement with the occurrence of extensive functionalization at the walls. Also remarkable is the broadness and increased intensity of the peak corresponding to the radial breathing mode appearing at 170 cm^{-1}.[19] The broadness of this peak is certainly unusual. We believe that this broadness derives from the specific characteristic of the **Py-SWNT** sample, particularly from the combination of short length and extensive wall functionalization (that could affect the breathing mode of the nanotubes to a larger extent than the functionalization occurring at the tips). In support of this rationalization, Figure 4 shows that the radial breathing mode peak of **pentyl ester-SWNT** remains sharp and with intensity similar to that of pristine purified SWNT. Combustion analyses of **Py-SWNT** were used to quantify the loading of pyridyl units, because functionalization introduces two nitrogen atoms per pyridyl isoxazoline unit. Thus, according to the nitrogen content, the estimated loading was 3.11 mmol of pyridyl units per gram of **Py-SWNT**.

For comparison, a fullerene having a covalently attached pyridyl unit connected through an isoxazoline ring linker (**Py-C_{60}**) was also prepared.[16] This fullerene derivative (**Py-C_{60}**) is very similar to the one previously reported for the study of photoinduced electron transfer of its **ZnPor** complex.[20] However, in the present case, the use of an isoxazoline ring as linker

(17) (a) Peng, H.; Alemany, L. B.; Margrave, J. L.; Khabashesku, V. N. *J. Am. Chem. Soc.* **2003**, *125*, 15174. (b) Dillon, A. C.; Yudasaka, M.; Dresselhaus, M. S. *J. Nanosci. Nanotechnol.* **2004**, *4*, 691. (c) Duesberg, G. S.; Blau, W. J.; Byrne, H. J.; Muster, J.; Burghard, M.; Roth, S. *Chem. Phys. Lett.* **1999**, *310*, 8. (d) Chen, J.; Rao, A. M.; Lyuksyutov, S.; Itkis, M. E.; Hamon, M. A.; Hu, H.; Cohn, R. W.; Eklund, P. C.; Colbert, D. T.; Smalley, R. E.; Haddon, R. C. *J. Phys. Chem. B* **2001**, *105*, 2525.
(18) (a) Saito, R.; Kataura, H. *Top. Appl. Phys.* **2001**, *80*, 213. (b) Saito, R.; Grueneis, A.; Samsonidze, G. G.; Dresselhaus, G.; Dresselhaus, M. S.; Jorio, A.; Cancado, L. G.; Pimenta, M. A.; Souza Filho, A. G. *Appl. Phys. A* **2004**, *A78*, 1099.
(19) Kukovecz, A.; Kramberger, Ch.; Holzinger, M.; Kuzmany, H.; Schalko, J.; Mannsberger, M.; Hirsch, A. *J. Phys. Chem. B* **2002**, *106*, 6374.
(20) D'Souza, F.; Smith, P. M.; Gadde, S.; McCarty, A. L.; Kullman, M. J.; Zandler, M. E.; Itou, M.; Araki, Y.; Ito, O. *J. Phys. Chem. B* **2004**, *108*, 11333.

Scheme 2. Chemical Structures of **Py-C_{60}**, **ZnPor**, and Their Corresponding Complexes with **ZnPor**, **ZnPor/Py-C_{60}**, and **ZnPor/Py-SWNT**

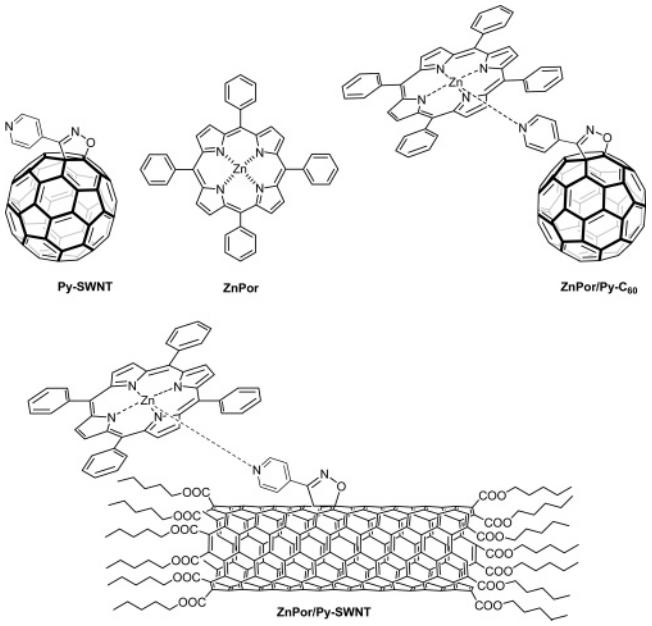

between the fullerene and the pyridyl moiety leads to a stronger electron-acceptor interaction when compared to the corresponding pyrrolidine linker analogue.[20] The corresponding complex **ZnPor/Py-C_{60}** was prepared by mixing **ZnPor** and the **Py-C_{60}**. As already mentioned, the main focus of this work was to establish the formation of a complex (**ZnPor/Py-SWNT**) between the pyridyl ring of functionalized **Py-SWNT** and the 5,10,15,20-tetraphenyl-21*H*,23*H*-porphine zinc (**ZnPor**) (Scheme 2). Complex **ZnPor/Py-C_{60}** was used as a model for the electrochemical and photophysical properties of **ZnPor/Py-SWNT**.

The formation of complex **ZnPor/Py-C_{60}** was demonstrated via ^{1}H NMR and UV−vis techniques. Figure 5 shows the ^{1}H NMR signals corresponding to the pyridyl protons in the spectrum of complex **ZnPor/Py-C_{60}**, which are shifted to 6.6 and 3.5 ppm. The corresponding protons of this group in fullerene derivative **Py-C_{60}** appear at 8.8 and 8.1 ppm. This fact has been used by other authors as evidence for the formation of a similar complex based on [60]fullerene and porphyrin.[7a,20]

The binding of **Py-C_{60}** to **ZnPor** results in the formation of the pentacoordinated zinc porphyrin via axial coordination. This process was monitored by recording the corresponding changes in UV−vis spectra of a solution of **ZnPor** in CH_2Cl_2 (5.6×10^{-5} M) upon addition of different amounts of **Py-C_{60}** (Figure 6). The formation of the pentacoordinated complex in dichloromethane was characterized by a slightly red-shifted Soret band and the appearance of an isosbestic point at 532 nm,[20] as shown in Figure 6. These spectral changes are in complete agreement with literature values for other fullerenes closely related to **Py-C_{60}**.

Analogously, formation of the supramolecular complex **ZnPor/Py-SWNT** between **ZnPor** and **Py-SWNT** was evaluated by ^{1}H NMR and UV−vis spectroscopy. Figure 7 shows the ^{1}H NMR spectra of **Py-SWNT** and complex **ZnPor/Py-SWNT**, in CD_2Cl_2. It can be clearly seen there that the protons corresponding to the pyridyl group are shifted to higher field for complex **ZnPor/Py-SWNT** as compared to the same protons

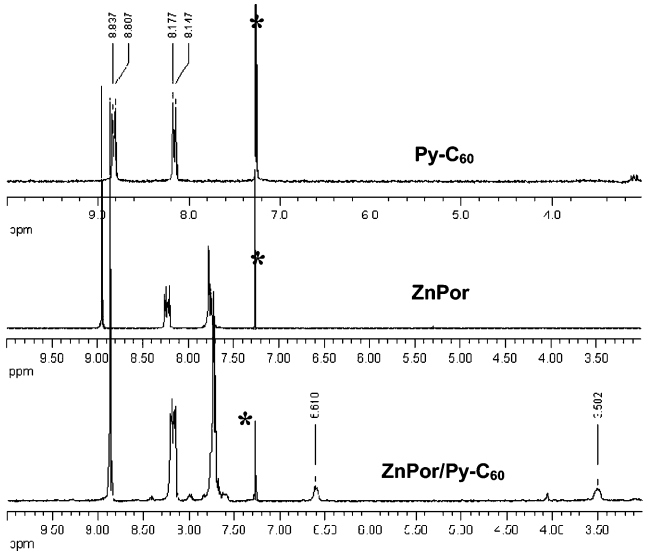

Figure 5. ^{1}H NMR spectra of compounds **Py-C_{60}**, **ZnPor**, and **ZnPor**/**Py-C_{60}** in $CDCl_3$. The signals due to the solvent have been marked with an asterisk.

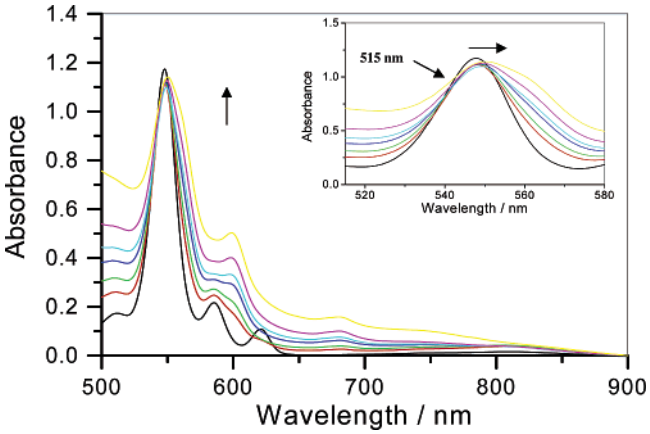

Figure 6. Absorption spectra of a solution of **ZnPor** (5.6×10^{-5} M in CH_2Cl_2) upon addition of increasing concentrations of **Py-C_{60}** (from 5.6×10^{-5} to 2.75×10^{-4} M). The arrow indicates the direction of **Py-C_{60}** concentration increases. The inset shows an enlargement of the visible bands in which the effect of complexation can be clearly seen.

in **Py-SWNT** similar to the observation for the fullerene complex **ZnPor**/**Py-C_{60}**. For the sake of clarity, we have labeled the chemical shift corresponding to the pyridyl protons in compound **Py-SWNT** and complex **ZnPor/Py-SWNT** (in Figure 7).

The UV−vis spectra showed that the addition of **Py-SWNT** to a solution of **ZnPor** in CH_2Cl_2 resulted in spectral changes characteristic of the presence of pentacoordinated **ZnPor**. The Soret and visible absorption bands of compound **ZnPor** were red-shifted as shown in Figure 8. This behavior follows the trend of what has been observed for the fullerene analogue, but the changes observed for **Py-SWNT** are significantly more pronounce.

To confirm that the pyridine group in **Py-SWNT** is involved in the coordination process, a control experiment using **pentyl ester-SWNT** was performed. No spectral changes were observed upon the titration of **ZnPor** with compound **pentyl ester-SWNT**, indicating no **ZnPor** coordination. Even though no spectroscopic changes were observed for the optical spectrum of **ZnPor** in the presence of **ester-SWNT**, we are aware of

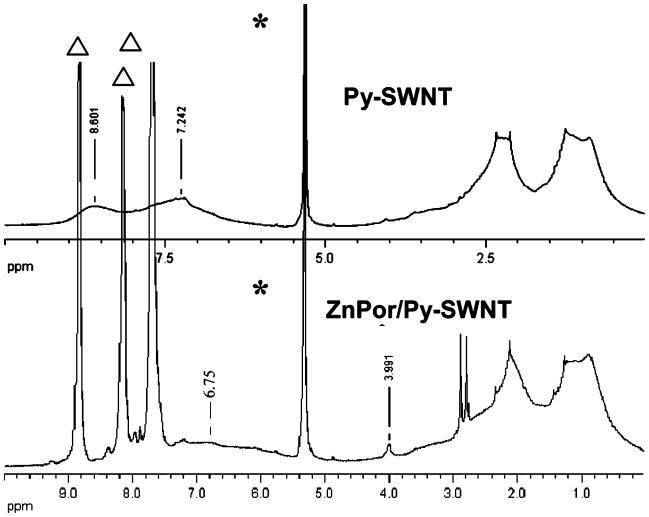

Figure 7. ^{1}H NMR spectra of **Py-SWNT** and **ZnPor/Py-SWNT** in CD_2Cl_2; the peaks attributed to the pyridyl group protons have been marked in the spectra. **ZnPor** and solvent signals have been marked with triangles and asterisks, respectively.

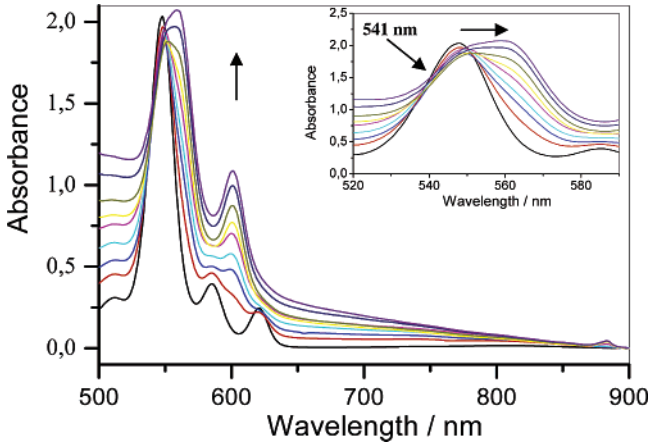

Figure 8. Absorption spectra of a solution of **ZnPor** (9.73×10^{-5} M in CH_2Cl_2) upon addition of increasing amounts of **Py-SWNT**. The arrows indicate the direction of **Py-SWNT** concentration increases. The inset shows an enlargement of the visible bands in which the effect of complexation can be clearly seen.

literature precedents[21] reporting that metalloporphyrins do interact with SWNT and that this interaction can be used for nanotube separation. In our case, however, the low concentrations of **ZnPor** and **pentyl ester-SWNT** used for optical spectroscopy measurements may be responsible for the lack of detectable interactions.

Electrochemical Studies

Cyclic voltammetric studies (CV) were performed to evaluate the electronic properties of the compounds and also to visualize the existence of any electronic interaction between **ZnPor** and **Py-C$_{60}$** and **Py-SWNT**, respectively.

The CV of **ZnPor** shows two oxidations and two reduction processes (see Supporting Information Figure S1). The first and the second reduction peaks are observed at −1.77 and −2.16 V versus Fc/Fc^+, respectively, and the values are reported in Table 1. The two oxidation processes are seen at +0.39 and +0.69 V, respectively.

Table 1. Redox Potentials (V vs Fc/Fc^+)[a] Determined by CV of Compounds **Py-C$_{60}$**, **ZnPor**, and the Different Mixtures of Compound **ZnPor** Titrated with **Py-C$_{60}$**

	oxidation		reduction		
compound	E_1	E_2	E_1	E_2	E_3
ZnPor	+0.39	+0.69	none	none	−1.77
Py-C60	none	none	−1.00	−1.39	−1.85
ZnPor + 0.5 equiv of **Py-C$_{60}$**	+0.36	+0.67	−1.13	−1.50	−1.96
ZnPor + 1.0 equiv of **Py-C$_{60}$**	+0.33	+0.70	−1.07	−1.45	−1.90
ZnPor + 1.5 equiv of **Py-C$_{60}$**	+0.32	+0.72	−1.07	−1.46	−1.90

[a] All potentials are half wave potentials unless indicated otherwise.

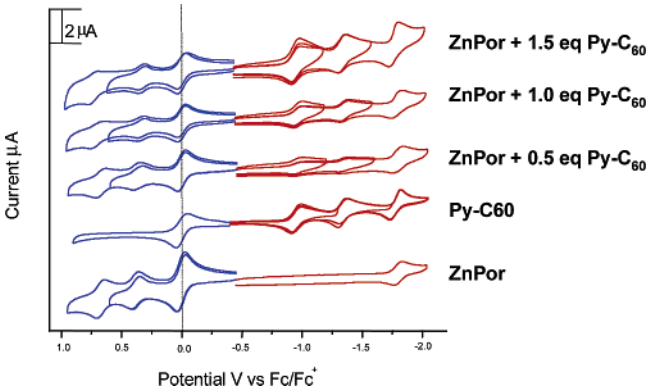

Figure 9. Comparative CVs of **ZnPor** and **Py-C$_{60}$** and the result of addition of 0.5, 1.0, and 1.5 equiv of **Py-C$_{60}$** to **ZnPor**.

The CV of **Py-C$_{60}$** shows the characteristic behavior of C_{60} derivatives (see Supporting Information Figure S2). The first three reduction processes are observed at −1.00, −1.39, and −1.85 V (Table 1), respectively, referenced versus the Fc/Fc^+ couple. The three processes are reversible. No oxidation peaks are observed within the potential window of the solvent.

Figure 9 shows the comparative CVs of **Py-C$_{60}$** and the result of addition of 0.5, 1.0, and 1.5 equiv of **Py-C$_{60}$** to **ZnPor** to form complex **ZnPor/Py-C$_{60}$**. Table 1 summarizes the observed potentials. The redox processes of complex **ZnPor/Py-C$_{60}$** correspond to those observed for the individual compounds (**ZnPor** and **Py-C$_{60}$**) but with some noticeable shifts.

The CV resulting from the addition of 0.5 equiv of compound **Py-C$_{60}$** to **ZnPor** shows that the first oxidation potential, which is based on the **ZnPor**, is shifted cathodically by about 30 mV to +0.36 V as compared to that of **ZnPor**. A similar shift is observed for the second oxidation potential, which now appears at +0.67 V. It is well known that nitrogenous bases will readily bind to metalloporphyrins having uncharged conjugated π systems.[22] Therefore, this shift indicates the formation of a complex via the axial coordination of the metal in the porphyrin with the nitrogen in the pyridyl group.

The first reduction process, which is fullerene based, also shifts cathodically by about 130 mV as compared to the first reduction potential of compound **Py-C$_{60}$**. The second reduction also shifts by about 110 mV to −1.5 V. The third reduction that appears to be an overlap between a porphyrin and a fullerenes-based redox process appears at −1.96 V. This corresponds to a shift of about 110 mV versus compound **Py-C$_{60}$** and 190 mV versus **ZnPor**. This further substantiates that both the fullerene as well as the porphyrin are affected upon complexation.

(21) Li, H.; Zhou, B.; Lin, Y.; Lingrong, G.; Wei, W.; Fernando, K. A. S.; Kumar, S.; Allard, L. F.; Sun, Y. *J. Am. Chem. Soc.* **2004**, *126*, 1014.

(22) Kadish, K. M.; Shiue, L. R.; Rhodes, R. K.; Bottomley, L. A. *Inorg. Chem.* **1981**, *20*, 1274.

Formation of the porphyrin−fullerene complex **ZnPor**/**Py-C$_{60}$** is also supported by additional shifts of the oxidation potential upon addition of larger quantities of fulleropyridine **Py-C$_{60}$**. On further addition for a total of 1.0 equiv of **Py-C$_{60}$**, the first oxidation shifts further by about 30 mV, thus resulting in a total cathodic shift of 60 mV, as compared to **ZnPor**. This again is due to complex formation. However, the second oxidation peak now shifts anodically by 30 mV instead of the earlier cathodic shift. The reduction processes show similar shifts in potentials. The first reduction process shifts anodically by 60 mV. The resultant shift from the first reduction of compound **Py-C$_{60}$** is 70 mV. A similar shift is seen in the second and third reductions, which now appear at −1.45 and −1.89 V, respectively. This is expected as further addition of compound **Py-C$_{60}$** results in the increase in concentration of free **Py-C$_{60}$** and the potential is an averaged value between the individual potentials of bound and unbound **Py-C$_{60}$**. Addition of a total of 1.5 equiv of compound **Py-C$_{60}$** shows a further 10 mV cathodic shift in the reduction potentials. Note that the trend in the first and the second oxidation peaks is opposite. Thus, while the first oxidation peak progressively decreases upon increasing fulleropyridine, the second peak first exhibits 20 mV decreases but then starts to shift to higher potentials. Probably the peak value measured in excess of fulleropyridine really corresponds to the oxidation potential of the complex **ZnPor**/**Py-C$_{60}$**, while the value observed under other conditions reflects the occurrence of a mixture of **ZnPor** and complex **ZnPor**/**Py-C$_{60}$** in different proportions. Thus, axial ligation results in complex formation between the functionalized fullerene and the zinc porphyrin, leading to noticeable shifts of the potentials for the complex with respect to those exhibited separately by both components.

An analogous electrochemical study was done with the SWNT derivative, **Py-SWNT**. **Py-SWNT** and its precursor **pentyl ester-SWNT** do not show any oxidation or reduction peaks. The CV displays cathodic currents beyond −0.6 V, which can be attributed to the reduction of soluble SWNTs as has been reported earlier (see Figure S3 in the Supporting Information for the CV of **Py-SWNT**).[17a]

Figure 10 shows the comparative CVs of **ZnPor** alone and with 0.5, 1.0, and 1.5 weight equivalents of **Py-SWNT**. Addition of 0.5 weight equivalents of **Py-SWNT** to a solution of **ZnPor** resulted in remarkable changes in the CV. All of the peaks undergo considerable broadening, and hence determination of half wave potentials was difficult. Thus, Osteryoung square wave voltammetry (OSWV) was used to determine the potentials. Table 2 lists the corresponding oxidation and reduction potentials.

The first oxidation peak of **ZnPor** that appeared at +0.39 V versus the ferrocene/ferrocenium couple shifted cathodically by almost 100 mV to +0.29 V. It is also seen that the second oxidation is composed of two individual processes, one at +0.53 V, and another at +0.69 V. The latter peak arises most probably from the second oxidation process of free **ZnPor**. Similarly, the first and second reduction potentials shifted cathodically by 90 and 40 mV and appear at −1.86 and −2.20 V, respectively.

Further addition of 0.5 weight equivalents of functionalized **Py-SWNT** results in an additional cathodic shift in the first oxidation by about 50 mV to +0.24 V. The second oxidation peak now appears at +0.52 V, and the peak seen earlier at +0.69 V disappears completely. The first and second reduction processes shift further cathodically to −1.90 and −2.23 V, which are shifts of 40 and 30 mV as compared to the previously observed values and a total of 130 and 70 mV as compared to free **ZnPor**. However, further addition of 0.5 weight equivalents of compound **Py-SWNT** had no effect on the potentials but led to broadening of the waves.

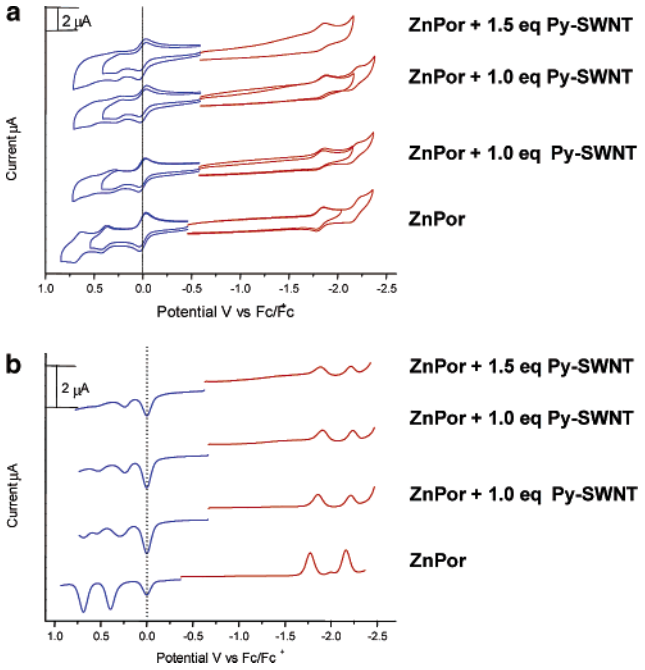

Figure 10. Comparative CV (a) and OSWV (b) plots of ZnPor and 0.5, 1.0, and 1.5 weight equivalents of Py-SWNT.

Table 2. Redox Potentials (V vs Fc/Fc$^+$) Determined by OSWV of **ZnPor** and the Different Mixtures of Compound **ZnPor** Titrated with **Py-SWNT**

	oxidation		reduction	
compound	E_1	E_2	E_1	E_2
ZnPor	+0.39	+0.69	−1.77	−2.16
ZnPor + 0.5 equiv of **Py-SWNT**	+0.29	+0.53	−1.86	−2.20
ZnPor + 1.0 equiv of **Py-SWNT**	+0.24	+0.52	−1.90	−2.23
ZnPor + 1.5 equiv of **Py-SWNT**	+0.24	+0.52	−1.89	−2.23

When the experiment was conducted by adding analogous quantities of the **pentyl ester-SWNT**, no shifts in redox potentials were observed, indicating that at the concentrations used in these experiments the shifts obtained were indeed due to complex formation and not due to noncovalent interactions between the porphyrins and the SWNTs.

The large shifts in oxidation and reduction potentials firmly support an interaction of the **Py-SWNT** with **ZnPor** via axial ligation of pyridyl units to the metal center.

Fluorescence Measurements

As expected on the basis of reports of **ZnPor** emission quenching by pyridyl-substituted fullerenes,[23] the presence of **Py-C$_{60}$** in benzonitrile quenched the emission of **ZnPor** (Figure 11a) with a quenching constant of 2.5×10^{12} $M^{-1}s^{-1}$ estimated

(23) (a) El-Khouly, M. E.; Gadde, S.; Deviprasad, G. R.; Fujitsuka, M.; Ito, O.; D'Souza, F. *J. Porphyrins Phthalocyanines* **2003**, *7*, 1. (b) D'Souza, F.; Deviprasad, G. R.; Zandler, M. E.; El-Khouly, M. E.; Fujitsuka, M.; Ito, O. *J. Phys. Chem. B* **2002**, *106*, 4952. (c) Armaroli, N.; Diederich, F.; Echegoyen, L.; Habicher, T.; Flamigni, L.; Marconi, G.; Nierengarten, J.-F. *New J. Chem.* **1999**, *23*, 77.

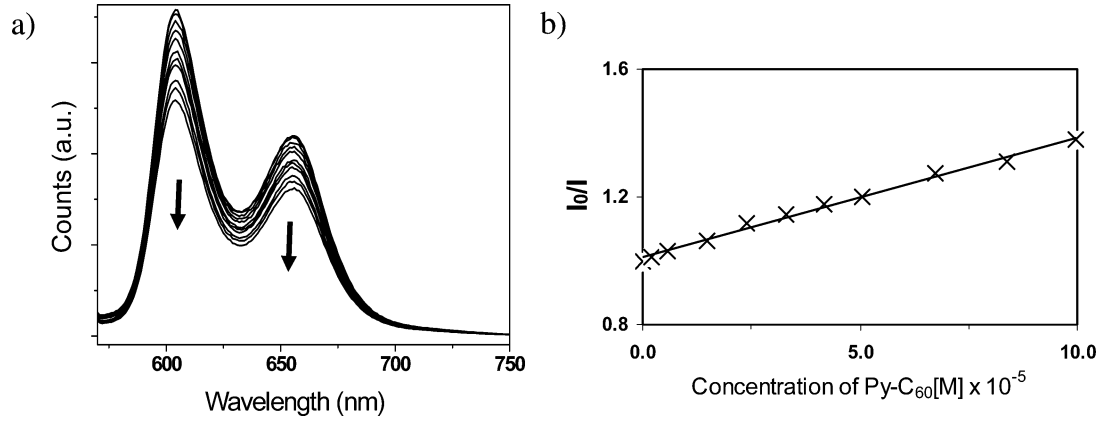

Figure 11. (a) Fluorescence spectra for a benzonitrile ($\lambda_{ex} = 560$ nm) solution of **ZnPor** (2×10^{-5} M) upon addition of increasing amounts of compound **Py-C_{60}** (concentration range $0-10^{-4}$ M). The arrows indicate the variation in the emission intensity upon increase of **Py-C_{60}** concentration. (b) Plot of the relative emission intensity measured at 600 nm versus the concentration of compound **Py-C_{60}**.

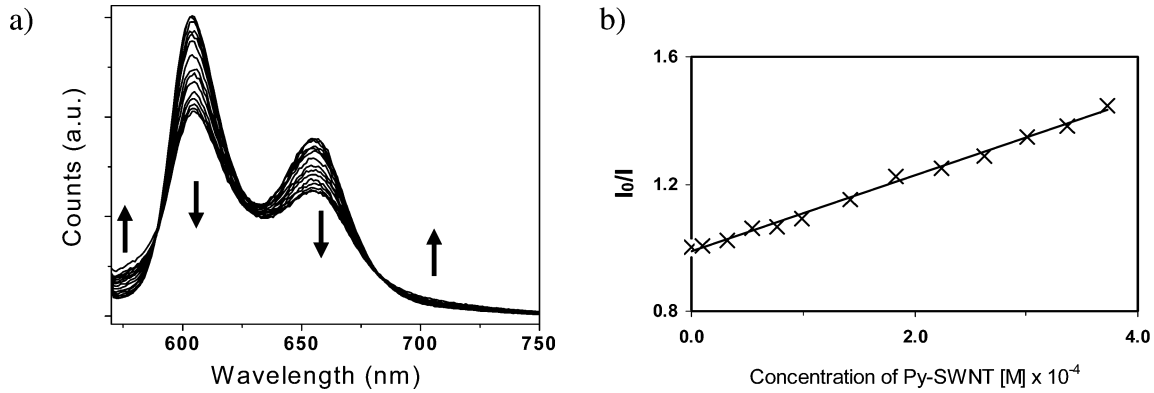

Figure 12. (a) Fluorescence spectra ($\lambda_{ex} = 560$ nm) for a benzonitrile solution of **ZnPor** (2×10^{-5} M) upon addition of increasing amounts of compound **Py-SWNT** (concentration from 0 to 3.8×10^{-4} M). The arrows in the figure indicate the relative variation of the bands upon increasing the **Py-SWNT** concentration. (b) Plot of the relative emission intensity measured at 600 nm versus the concentration of compound **Py-SWNT**. This concentration refers to the moles of pyridyl groups attached to SWNT per liter.

from a Stern−Volmer plot (Figure 11b). This quenching rate constant for the emission of **ZnPor** by the fullerene derivative is about 2 orders of magnitude higher than the diffusion rate constant in most common solvents. Thus, this high quenching rate constant probably reflects the contribution of static quenching to the fluorescence intensity decrease. Static quenching occurs when formation of a complex prior to light excitation occurs, causing the immediate deactivation of the fluorophore. In other words, preassociation between the quencher and the fluorophore leads to an apparent quenching rate constant that is higher than that expected for a diffusion-controlled process.[24] In fact, this complex formation is the case between compound **Py-C_{60}** and **ZnPor** to form complex **ZnPor/Py-C_{60}**.

Interestingly, the **ZnPor** emission quenching caused by compound **Py-C_{60}** does not lead to the observation of the fullerene emission that would appear at 700−900 nm, thus suggesting that the emission quenching occurs through a photoinduced electron-transfer mechanism, as previously reported by Ito and co-workers for a closely related system.[28a,b]

Addition of increasing amounts of compound **Py-SWNT** also quenches the **ZnPor** emission due to the interaction between **ZnPor** and **Py-SWNT**, leading to complex formation. Comparison of the singlet excited-state quenching rate constant of **ZnPor** by **Py-SWNT** and **Py-C_{60}** is complicated by the fact that compound **Py-C_{60}** is a discrete molecule; functionalized **Py-SWNT** has multiple pyridyl groups. Therefore, rather than a bimolecular quenching constant, it is better to normalize the data to the concentration of pyridyl groups present in the solution. When the quenching rate constant per pyridyl group is calculated, pyridyl groups of **Py-C_{60}** are better quenchers than pyridyl groups attached to the SWNT. This is not surprising considering that in the case of **Py-SWNT**, all of the pyridyl groups are bonded to the same scaffold and they are not free to diffuse independently. A value for the Stern−Volmer quenching rate constants was obtained on the basis of the density of pyridyl groups determined by combustion elemental analysis, to give Ksv 7.9×10^{11} M^{-1}, which is also "similar" to the Ksv determined for the **Py-C_{60}** (Ksv 2.5×10^{12} M^{-1}). Importantly, while quenching with pyridyl-fullerene (**Py-C_{60}**) does not allow the observation of any new emission, Figure 12 shows that in addition to a decrease of the **ZnPor** emission, the presence of **Py-SWNT** gives rise to the concurrent increase of a very broad

(24) Lakowicz, J. R. *Principles of Fluorescence Spectroscopy*; 1983.
(25) Alvaro, M.; Atienzar, P.; Bourdelande, J. L.; Garcia, H. *Chem. Commun*. **2002**, 3004.
(26) (a) Fraser, D. D.; Bolton, J. R. *J. Phys. Chem.* **1994**, *98*, 1626. (b) Levin, P. P.; Batova, E. E.; Shafirovich, V. Y. *Chem. Phys.* **1990**, *142*, 279. (c) Shafirovich, V. Y.; Batova, E. E.; Levin, P. P. *Chem. Phys.* **1992**, *162*, 155.
(27) (a) Togashi, D. M.; Costa, S. M. B. *Phys. Chem. Chem. Phys.* **2002**, *4*, 1141. (b) Furuto, T.; Lee, S. K.; Amao, Y.; Asai, K.; Okura, I. *J. Photochem. Photobiol., A* **2000**, *132*, 81.
(28) (a) Harada, A.; Yamaguchi, H.; Okamoto, K.; Fukushima, H.; Shiotsuki, K.; Kamachi, M. *Photochem. Photobiol.* **1999**, *70*, 298. (b) Rajesh, C. S.; Capitosti, G. J.; Cramer, S. J.; Modarelli, D. A. *J. Phys. Chem. B* **2001**, *105*, 10175.

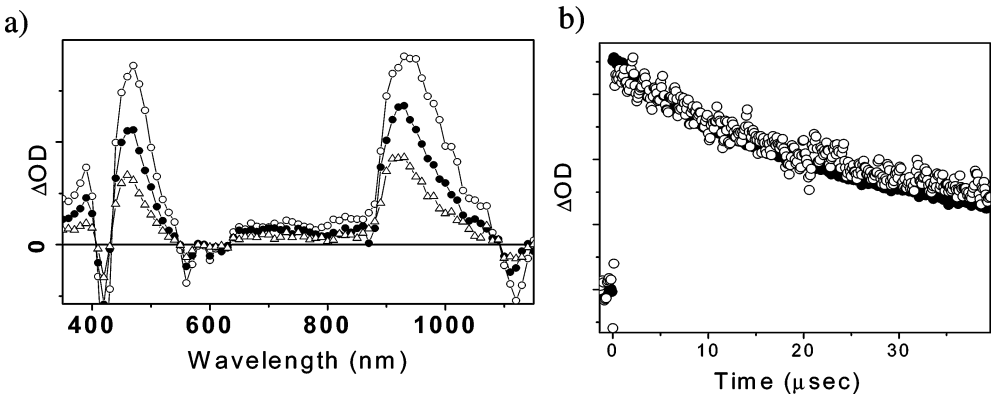

Figure 13. (a) Transient spectra recorded at 2 (○), 30 (●), and 80 (△) μs after 355 nm laser excitation of a N_2-purged benzonitrile solution of **ZnPor** (2×10^{-5} M). (b) Signal decay monitored at 470 (●) and 940 nm (○).

emission. We observed clear isoemissive points at 580 and 680 nm that indicate that the growth of the new emission occurs at the expense of the **ZnPor** emission decrease. These features indicate in the case of **Py-SWNT** an energy transfer process. To investigate this further, the emission of **Py-SWNT** upon direct excitation at 390 nm was recorded.

Upon 390 nm excitation of a N_2-purged benzonitrile solution of compound **Py-SWNT**, a broad emission spectrum between 400 and 700 nm was observed (see Figure S4 in the Supporting Information for the emission spectrum of **Py-SWNT**). This type of fluorescence emission spectrum has also been observed for pristine and unfunctionalized SWNT,[25] and it is believed to arise from excitation of nanotube defects having local structures analogous to condensed polycyclic aromatic compounds.

On the basis of the existence of **Py-SWNT** emissive excited states, the most likely explanation for the origin of the new emission when observing the emission of **ZnPor** is an energy transfer from the singlet excited state of **ZnPor** to **Py-SWNT**. Emissive excited states of **Py-SWNT** are populated, and they are responsible for the emission increase observed in Figure 12. These excited states of **Py-SWNT** can be different from those reached upon direct excitation at 390 nm. Attempts to observe emission from **Py-SWNT** after exciting at the long wavelengths used for **ZnPor** excitation failed. Thus, blank controls even at a **Py-SWNT** concentration of 3.8×10^{-4} M did not show any detectable emission when directly excited at 560 nm. These blank experiments clearly confirm that the luminescence observed in Figure 12 really originated by photosensitization from **ZnPor** and not from direct excitation of compound **Py-SWNT** at 560 nm.

To characterize the nature of the transients generated in the quenching of **ZnPor** by compounds **Py-SWNT** and **Py-C_{60}**, a laser flash photolysis study was performed. Starting with a solution of **ZnPor** in benzonitrile or DMF and in agreement with literature data,[26] upon 355 nm laser flash excitation a transient spectrum with absorption bands at 470 and 930 nm was recorded (Figure 13). This transient was assigned to the triplet excited state of **ZnPor** on the basis of literature reports.[27] In agreement with the triplet nature of this excited state, oxygen quenches the signal without the appearance of any new transient. The spectrum also contains negative signals at 430, 560, and 600 nm corresponding to bleaching of the porphyrin ground state.

Kinetic analysis of the signal profile at different wavelengths shows that these peaks correspond to a single transient whose

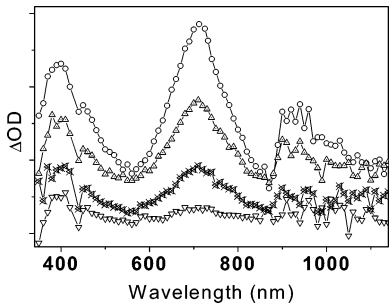

Figure 14. Transient spectra recorded at 2 (○), 30 (△), 50 (×), and 80 (▽) μs after 355 nm laser excitation of a N_2-purged benzonitrile solution of **ZnPor** (2×10^{-5} M) upon addition of compound **Py-C_{60}** (3×10^{-4} M).

Scheme 3. Quenching Mechanism of **ZnPor** with **Py-C_{60}**[a]

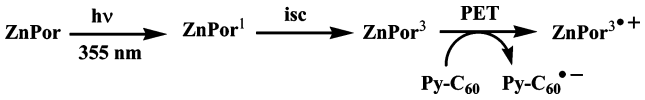

[a] isc, intersystem crossing; PET, photoinduced electron-transfer quenching.

decay matches reasonably well the recovery of the ground absorption (Figure 12). The triplet signal decay was fitted to a monoexponential kinetic process with a lifetime of 36 and 25 μs in benzonitrile and DMF, respectively. The signal corresponding to the triplet excited state of **ZnPor** was quenched by **Py-C_{60}** with an apparent quenching rate constant of 5.1×10^8 s^{-1} M^{-1} obtained from the plot of the observed monoexponential decay rate constants versus **Py-C_{60}** concentration (see Figure S5 in the Supporting Information). When the concentration of compound **Py-C_{60}** was sufficiently high, the transient spectrum changed and the initial peaks of the triplet excited state were replaced by absorption peaks at 410, 700, and 940 nm, indicating the formation of some different transients (Figure 14).

These spectral changes are compatible with the occurrence of a photoinduced electron transfer from the triplet excited state of **ZnPor** to **Py-C_{60}**, giving rise to **ZnPor**$^{\bullet+}$ (peaks at 400 and 700 nm) and the radical anion of **Py-C_{60}** (structured absorption 900−1100 nm) according to Scheme 3. The λ_{max} values observed for these species are in agreement with literature data for the same or similar transients.[28]

At this high concentration, the half-life of the **ZnPor**$^{\bullet+}$, measured a 710 nm, was estimated by fitting the time profile of the signal to a single-exponential decay, giving a half-life of 7.5 μs.

The lifetime of the **Py-$C_{60}^{\bullet-}$** radical anion was, on the other hand, estimated from the decay of the signal monitored at 910 nm, giving a half-life of 26 μs, significantly longer-lived than **ZnPor$^{\bullet+}$** (see Figure S6 in the Supporting Information for the actual signal decays of **ZnPor$^{\bullet+}$** and **Py-$C_{60}^{\bullet-}$**). These differences in the lifetimes suggest that the decays monitored in the microsecond time scale do not correspond to the back electron-transfer annihilation from **Py-$C_{60}^{\bullet-}$** to **ZnPor$^{\bullet+}$** to form the initial ground states. Most probably, the radical ions monitored correspond to solvent-separated radical ions.

In contrast to the behavior observed for compound **Py-C_{60}** that quenches both singlet (fluorescence studies) and triplet excited states (laser flash experiments) of **ZnPor**, the presence of increasing amounts of **Py-SWNT** in the range 10−100 μM (based on the concentration of pyridyl groups per gram of **Py-SWNT**) does not affect the triplet excited state of **ZnPor** when the study is conducted in benzonitrile. However, working in DMF, which is a more polar and less coordinating solvent than benzonitrile, some quenching of the **ZnPor** triplet was observed, accompanied by a decrease in **ZnPor** triplet signal intensity. This solvent effect on the **ZnPor** triplet can be explained considering that the singlet excited state of **ZnPor** is quenched by **Py-SWNT** with a higher quenching rate constant than that for the triplet and quenching of the **ZnPor** triplet excited state may or may not occur depending on solvent polarity and solvent coordination ability. Analogously to what has been observed here for **Py-SWNT**, there are sufficient reports in the literature showing that in the case of fullerene-derived dyad and triad, the polarity of the solvent plays a decisive role in controlling the ratio between energy and electron transfer, the quantum yield for charge separation, and the lifetime of the charge-separated state.[29] Thus, **Py-SWNT** quenches the fluorescence of **ZnPor** and reduces the intensity of the photogenerated triplets. On the other hand, the influence of **Py-SWNT** on the triplet decay kinetics allowed estimation for the quenching rate constant of compound **Py-SWNT** in DMF at 5.36×10^7 M^{-1} s^{-1}. This value is significantly lower than the one determined for the quenching with compound **Py-C_{60}**. Furthermore, even at high concentrations of **Py-SWNT** in the range of 10−100 μM, no changes in the transient absorption spectrum of **ZnPor** triplets other than an intensity decrease and a shorter lifetime were observed, and thus the only transient that is being detected in these laser experiments corresponds to the **ZnPor** triplets excited state.

There are remarkable differences in the influence of **Py-C_{60}** and **Py-SWNT**, in the photophysics of **ZnPor**. While compound **Py-C_{60}** interacts with the excited state of **ZnPor** through a photoinduced electron-transfer mechanism, giving rise to the corresponding **Py-$C_{60}^{\bullet-}$** radical anion, no evidence for an analogous process could be observed for compound **Py-SWNT**. In the latter case, it seems that singlet excited and triplet states are most probably quenched through an energy transfer mechanism. Observation of emission from **Py-SWNT** upon excitation of **ZnPor** supports the occurrence of energy transfer photosensitization. This contrasting behavior between pyridyl-substituted fullerene and SWNT can be easily rationalized considering that the C_{60} core is the electron acceptor (see Table 1 for redox potentials). Thus, it is not surprising that **Py-SWNT** does not abstract one electron from the **ZnPor** excited state while **Py-C_{60}** does. Concerning earlier work reporting photoinduced electron transfer between metalloporphyrins and modified SWNT attached either not covalently[9] or covalently,[30] in our case the lack of observation of photoinduced electron transfer for the **ZnPor/Py-SWNT** complex indicates that the structure of the supramolecular entity and the actual nature of the linkage between **ZnPor/Py-SWNT** plays a decisive role governing the fate of the electronic excited state.

Conclusions

A highly soluble SWNT derivative being functionalized at the tips with pentyl esters and on the walls by pyridyl isoxazoline groups has been prepared and characterized. Particularly interesting are the TEM images showing the short length of the tubes and the solution ^{1}H NMR showing the presence of corresponding adducts. Raman spectroscopy showed the expected peaks for the organic groups and confirmed the occurrence of a high degree of lateral functionalization. This pyridyl-functionalized SWNT forms complexes with **ZnPor** in a way parallel to that of the pyridyl-derivatized C_{60}. The occurrence of this complex is clearly revealed by optical spectroscopy and by the shifts in CV potentials of **ZnPor** in the presence of **Py-SWNT**, similar but larger than for the corresponding fullerene analogues. Steady-state fluorescence and nanosecond transient spectroscopy indicates an energy transfer quenching of the **ZnPor** singlet excited state by **Py-SWNT** and no evidence for the occurrence of electron transfer.

Experimental Section

General Information. ^{1}H NMR spectra were recorded in $CDCl_3$ on a 200 MHz apparatus. UV−vis absorption spectra were obtained in acetonitrile using quartz cuvettes on a Shimadzu spectrophotometer. FT-IR spectra were recorded on a Nicolet Impact 410 spectrophotometer using KBr disks or self-supported wafers (**Py-SWNT**) compressed to 2 Ton × cm^{-2} for 2 min. Photoluminescence measurements were performed in acetonitrile solution at room temperature in N_2-purged septum-capped quartz cells using an Edinburgh FL3000 spectrofluorometer, a Xe-doped mercury lamp, and a Czerny-Turner monochromator. Laser flash photolysis experiments were carried out using the third (355 nm) harmonic of a *Q*-switched Nd:YAG laser (Spectron Laser Systems, UK; pulse width ca. 9 ns and 35 mJ × $pulse^{-1}$). The signal from the monochromator/photomultiplier detection system was captured by a Tektronix TDS640A digitizer and transferred to a PC computer that controlled the experiment and provided suitable processing and data storage capabilities.

The electrochemical measurements for all compounds were performed with a BAS 100B Electrochemical Workstation. Here, 0.1 M tetrabutylammonium hexafluorophosphate ($TBAPF_6$, from Fluka) in CH_2Cl_2 was used as the supporting electrolyte (degassed with argon saturated with CH_2Cl_2 vapors). A platinum wire was employed as the counter electrode, and an Ag wire was used as the reference electrode. Ferrocene (Fc) was added as an internal reference, and all of the potentials were referenced relative to the Fc/Fc^+ couple. A glassy carbon electrode (CHI, 0.5 mm in diameter), polished with 0.3 μm aluminum paste and ultrasonicated in deionized water and CH_2Cl_2 bath, was used as the working electrode. The scan rates for CV were 100 mV. The OSWV was performed with potential steps of 4 mV; a square wave amplitude of 25 mV at a frequency of 15 Hz was applied. Experiments were performed at room temperature (20 ± 2 °C).

(29) Pérez, L.; García-Martínez, J. C.; Díez-Barra, E.; Atienzar, P.; García, H.; Rodríguez-López, J.; Langa, F. *Chem.-Eur. J.*, in press.

(30) Baskaran, D.; Mays, J. W.; Zhang, X. P.; Bratcher, M. S. *J. Am. Chem. Soc.* **2005**, *127*, 6916.

Synthesis of Pentyl Ester-SWNT. A purified HiPco SWNT sample (Carbolex 50 mg) was treated with a concentrated HCl solution to recover all of the carboxylic acid groups in the nanotube, followed by refluxing in thionyl chloride (2 mL) for 24 h to convert the carboxylic acids into acyl chlorides. Thionyl chloride was removed by washing with anhydrous THF, and the solvent was evacuated under reduced pressure. The acyl chloride nanotube was then mixed in a flask with 2 g of *n*-pentanol, and the resulting solution was heated to 80 °C and stirred for 72 h under argon. The excess of *n*-pentanol was removed by vacuum distillation. The residue was extracted several times with chloroform to obtain a dark brown solution that was filtered (Swinney Millipore 0.2 μm filter) to ensure separation from nonsoluble SWNT. The solvent was removed on a rotary evaporator yielding the **pentyl ester-SWNT** (22 mg). ^{1}H NMR ($CDCl_3$): δ 3.80 (bs), 2.19 (bs), 1.28 (bs), 0.89 (bs). UV−vis (CH_2Cl_2): λ_{max}/nm 229.

Synthesis of Compound Py-SWNT. To a solution of 4-pyridylcarboxaldehyde oxime (**1**), in 40 mL of anhydrous chloroform, was added 0.01 mL of anhydrous pyridine. The solution was cooled at 0 °C, *N*-chlorosuccinimide (3.5 mmol) was added, and the mixture was stirred for 15 min. The solvent was removed, and a solution of compound **pentyl ester-SWNT**[15] (30 mg) and triethylamine in *o*-dichlorobenzene was added to the solid. The mixture was irradiated in a focused microwave oven at 150 W for 45 min. The solvent was distilled, and the solid was purified by washing several times with chloroform/water, chloroform/ethyl ether, and chloroform/pentane, yielding compound **Py-SWNT** (20 mg). IR (ATR) ν/cm^{-1}: 2930, 1700, 1630. ^{1}H NMR ($CDCl_3$): δ/ppm 8.65 (bs), 7.25 (bs), 3.7 (bs), 2.4 (bs), 2.1 (bs), 1.3 (bs), 0.9 (bs). UV−vis (CH_2Cl_2) λ_{max}/nm: 233. The amount of pyridyl groups **Py-SWNT** was estimated from the comparison of the combustion chemical analysis data of nitrogen for **Py-SWNT** (carbon, 74.32 wt % and nitrogen, 5.71 wt %), assuming that all of the nitrogen content corresponds to pyridyl-isoxazoline substituents. Thermogravimetric analysis under an air stream of pristine, pentyl esterified, and **Py-SWNT** shows in all cases that the material completely disappears at temperatures below 600 °C.

Acknowledgment. Financial support by the Spanish Ministerio de Educación y Ciencia (MAT 2003-01226, CTQ2004-00364/BQU, and FEDER funds), the Junta de Comunidades de Castilla-La Mancha (Project PAI-05-068), and Generalidad Valenciana (GV Grupos 03-020) is gratefully acknowledged. P.A. also thanks the Spanish Ministry for a postgraduate scholarship. L.E. and A.P. thank the chemistry division of the US NSF for generous financial support (CHE-0509989).

Supporting Information Available: Cyclic voltammograms, fluorescence spectra, and graphs of signal decay. This material is available free of charge via the Internet at http://pubs.acs.org.

JA057742I